arXiv:1212.4000v2 [quant-ph] 20 Dec 2012

Stabilizer quantum error correction toolbox for superconducting qubits

Simon E. Nigg and S. M. Girvin
Department of Physics, Yale University, New Haven, CT 06520, USA

(Dated: December 21, 2012)

We present a general protocol for stabilizer measurements in a system of N superconducting qubits. We assume always-on, equal dispersive couplings χ to a single mode of a high-Q microwave resonator in the ultra-strong dispersive limit defined by $\chi \gg 1/T_2, \kappa$, where T_2 is the qubit coherence time and κ is the cavity linewidth. In this limit, we show how to map the two eigenvalues of an arbitrary weight $M \leq N$ Pauli operator, onto two quasi-orthogonal coherent states of the cavity. Together with a fast cavity readout ($T_{\mathrm{meas}} \ll 1/\kappa$), this enables the efficient measurement of stabilizer operators.

Several milestones on the road to quantum computing with superconducting circuits have recently been reached, such as the experimental demonstrations of Shor's factorization algorithm [1] and of rudimentary quantum error correction (QEC) [2]. As the resources required for more complete QEC protocols get within experimental reach, it is desirable to develop a toolbox sufficiently versatile to allow the implementation of a wide class of codes. Most QEC codes can be described concisely in the stabilizer formalism of Gottesman [3]. In this framework a QEC code is defined by the subspace spanned by the eigenstates with eigenvalue +1 of a set of commuting multi-qubit Pauli operators called stabilizers. Error detection is achieved by measuring the stabilizers of the code; the syndrome of an error being a sign flip of stabilizers. Correction in turn, can be performed when the collection of syndromes contains enough information to identify the location and type of the error. The ability to measure arbitrary multi-qubit Pauli operators would thus allow a direct realization of stabilizer QEC codes.

Recent dramatic progress in coherence times for superconducting qubits coupled to 3D cavities [4–6], has inspired new theoretical ideas for mapping qubit states to Schrödinger cat cavity states [7, 8]. Following, these developments, we show in this work, how to realize stabilizer measurements with superconducting qubits coupled off-resonantly to a common mode of a high-Q cavity. Advantages of our approach over previous proposals [9, 10] include a simpler hardware and the ability to selectively address an arbitrary subset of qubits, without the need for tunable couplings. Besides its relevance for stabilizer QEC, our approach paves the way for the preparation of arbitrary cluster states for measurement-based quantum computation [11] and for the digital simulation of quantum lattice models with non-trivial topology such as the toric and surface codes [12, 13], similar to a recent work on trapped ions [14].

Central to our proposal is the off-resonant coupling between a superconducting qubit and a single mode of a microwave resonator [15] described by the dispersive Hamiltonian $H_{\mathrm{disp}} = \chi \boldsymbol{\sigma}^z \boldsymbol{a}^\dagger \boldsymbol{a}$, where $\boldsymbol{\sigma}^z = |e\rangle\langle e| - |g\rangle\langle g|$ is the Pauli matrix in the computational basis $\{|g\rangle, |e\rangle\}$ of the qubit and $\boldsymbol{a}$ ($\boldsymbol{a}^\dagger$) denotes the photon annihilation (creation) operator of the cavity mode. This coupling describes a qubit-state-dependent frequency shift $\pm\chi$ of the cavity, or equivalently a photon-number-dependent frequency shift $2n\chi$ of the qubit. In the weakly dispersive regime $1/T_2, \kappa \sim 2\chi$, where κ is the bare cavity linewidth and $T_2^{-1} = (2T_1)^{-1} + \Gamma_\phi$ is the qubit coherence time composed of relaxation $1/T_1$ and pure dephasing Γ_ϕ, this interaction has been used for a qubit-readout by measuring the phase-shift of transmitted or reflected microwaves [15]. In the strong dispersive regime $1/T_2, \kappa < 2\chi$, the same interaction can be used to resolve different photon numbers in the qubit spectrum [16]. In this work, we are interested in the ultra-strong dispersive regime, where $\kappa, 1/T_2 \ll \chi$. In this regime, it becomes possible, by using microwave pulses narrow in frequency compared with χ but large compared with κ and $1/T_2$, to perform qubit rotations conditioned on the number of photons in the cavity, or cavity displacements conditioned on the state of the qubit [7, 8]. Here we show how to take advantage of this novel regime to encode the two eigenvalues of an arbitrary multi-qubit Pauli operator onto quasi-classical oscillations of light that differ in phase by π.

Although our scheme is applicable to other types of superconducting qubits, for clarity we will frame our discussion around the specific case of transmon qubits. A transmon qubit [4, 17] is formed by a superconducting dipole-antenna with a Josephson junction at its center with Josephson energy $E_J \gg E_C \equiv e^2/(2C_\Sigma)$, where C_Σ represents the total capacitance between the antenna pads. Neglecting charge-dispersion effects, which are suppressed exponentially in E_J/E_C [17], the low-energy spectrum of an isolated transmon is well approximated by that of an anharmonic oscillator with frequency $\omega_{01} \approx \sqrt{8E_J E_C} - E_C$ and weak anharmonicity $\omega_{01} - \omega_{12} \approx E_C \ll \omega_{01}$. In state-of-the-art realizations, the qubit linewidth $1/T_2$ is close to being limited by relaxation [4, 18–20]. In this work we are interested in a setup such as depicted in Fig. 1 (a), where N transmons are coupled dispersively to a microwave field inside a 3D cavity. For control and readout purposes, an ancilla qubit, is further dispersively coupled to both the high-Q cavity containing the N qubits with $\chi_A \gg N\chi$ and to a

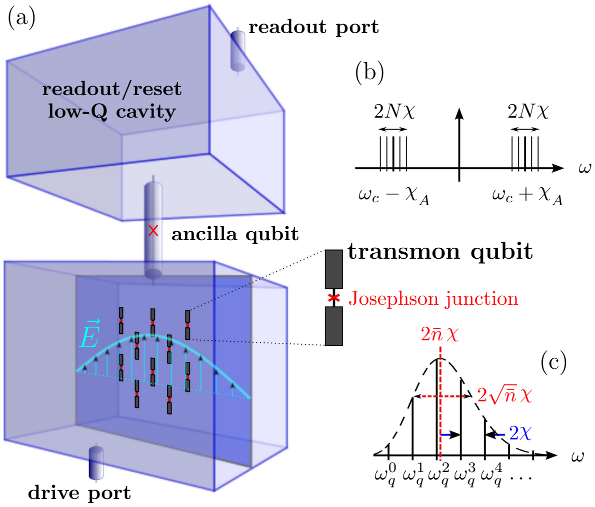

FIG. 1. (Color online) **(a)** 2D array of N transmon qubits in a 3D cavity. The ancilla qubit and the upper cavity are used for readout/reset and manipulation purposes. Cavity **(b)** and qubit **(c)** spectra in the ultra-strong dispersive regime.

low-Q (readout) cavity, similar to the setup used in [6]. We assume that both the ancilla qubit and the readout cavity remain in the ground state, except during readout and manipulation. Thus omitting, for now, the corresponding degrees of freedom, we model this system in an appropriately rotating frame (see supplemental material for details), by the effective Hamiltonian

$$H_0 = \chi \sum_{i=1}^{N} \boldsymbol{\sigma}_i^z \boldsymbol{a}^\dagger \boldsymbol{a} - K \boldsymbol{a}^\dagger \boldsymbol{a}^\dagger \boldsymbol{a}\boldsymbol{a}\,. \tag{1}$$

The transmons are treated here as two-level systems assuming their anharmonicity is larger than their linewidth (i.e. $E_C > 1/T_2$). Furthermore, we neglect the cavity-mediated qubit-qubit interaction, assuming the qubits to be sufficiently detuned from each other. Crucially, we require the N qubits inside the cavity to have equal dispersive coupling χ with the cavity mode. In practice this may require some fine-tuning of the individual qubit transition frequencies and coupling strengths. The frequencies could be tuned for example by using split-Josephson junctions for each transmon and flux-bias lines to control their effective Josephson energy [21], while the coupling strengths could be adjusted through the geometry and placement of the transmons in the cavity. The second term on the rhs of Eq. (17) accounts for the (negative) qubit-induced anharmonicity of the cavity [22, 23]. In the weak and strong dispersive regimes, this term can usually be neglected as $K \ll \chi$. We find that in the ultra-strong dispersive regime it is necessary to account for its leading order effect. We next show how to encode the parity $\boldsymbol{Z}_{S_N} = \bigotimes_{i=1}^{N} \boldsymbol{\sigma}_i^z$ of an N-qubit state $|\psi\rangle_N$ onto two quasi-orthogonal coherent states of the cavity differing in phase by π.

Parity encoding. Suppose the system is initially prepared in the product state $|\Psi\rangle_{t=0} = |\alpha\rangle|\psi\rangle_N$, where $|\alpha\rangle$ is a coherent state of the cavity with amplitude α. Making use of the identity $\exp[-i(\pi/2)\sum_{i=1}^{N}\boldsymbol{\sigma}_i^z] = (-i)^N \boldsymbol{Z}_{S_N}$, one can show that under the action of (17), at time $T = \pi/(2\chi)$, the state becomes

$$|\Psi\rangle_T = \boldsymbol{U}_K \left(|\alpha_N\rangle \boldsymbol{P}_{S_N}^{+} + |-\alpha_N\rangle \boldsymbol{P}_{S_N}^{-}\right)|\psi\rangle_N, \tag{2}$$

where $\boldsymbol{P}_{S_N}^{\pm} = (\mathbb{1} \pm \boldsymbol{Z}_{S_N})/2$ are the projectors onto the even $(+)$ and odd $(-)$ qubit parity subspaces as measured by the ± 1 eigenvalues of the multi-qubit Pauli operator $\boldsymbol{Z}_{S_N}$ and $\alpha_N = (-i)^N \alpha$. Note that the self-Kerr term is qubit-independent [24] and conserves the photon number $\boldsymbol{a}^\dagger \boldsymbol{a}$. Because it commutes with the dispersive term, its effect factors out and is captured in (19) by the unitary operator $\boldsymbol{U}_K = \exp[i\pi K/(2\chi)\boldsymbol{a}^\dagger\boldsymbol{a}^\dagger\boldsymbol{a}\boldsymbol{a}]$. For weak nonlinearity such that $\pi K \ll \chi$, the leading order effect of $\boldsymbol{U}_K$ acting on the coherent states $|\pm\alpha_N\rangle$ is a rotation of the mean amplitude by an angle $\Delta\phi_{\rm nl} = \pi\bar{n}K/\chi$ with the mean photon number $\bar{n} = |\alpha|^2$. To leading order in K/χ, the state (19) is thus well approximated by

$$|\Psi\rangle_T = |\tilde{\alpha}_N\rangle \boldsymbol{P}_{S_N}^{+}|\psi\rangle_N + |-\tilde{\alpha}_N\rangle \boldsymbol{P}_{S_N}^{-}|\psi\rangle_N\,, \tag{3}$$

with $\tilde{\alpha}_N = \alpha_N e^{i\Delta\phi_{\rm nl}}$. The sub-leading order effect is a damping of the mean amplitude by a factor $\exp(-\Delta\phi_{\rm nl}^2/(2\bar{n}))$ [25]. We emphasize that in the ultra-strong dispersive regime $\kappa/\chi \ll 1$ considered here, photon decay only weakly damps the amplitude of the coherent states in (12) by a factor $\exp(-\kappa T/2) \approx 1 - (\pi/4)(\kappa/\chi)$. Ignoring these small effects, we thus see that the dispersive interaction can be used to encode the parity of the multi-qubit state onto two coherent states of the cavity differing in phase by π.

Subset selectivity. Often stabilizers are defined on subsets of qubits. Selectivity to $M \leq N$ qubits, labeled by the set $S_M \subseteq S_N = \{1, \ldots, N\}$, can be achieved as follows. Consider the identity

$$\boldsymbol{U}_{S_M}(t) = \Big(\bigotimes_{i\in S_M^c} \boldsymbol{\sigma}_i^x\Big)\boldsymbol{U}_{S_N}\Big(\frac{t}{2}\Big)\Big(\bigotimes_{i\in S_M^c} \boldsymbol{\sigma}_i^x\Big)\boldsymbol{U}_{S_N}\Big(\frac{t}{2}\Big), \tag{4}$$

where $\boldsymbol{U}_S(t) = \exp(-it\chi\boldsymbol{a}^\dagger\boldsymbol{a}\sum_{i\in S}\boldsymbol{\sigma}_i^z)$ and $S_M^c = S_N \backslash S_M$ is the complement set to S_M. Eq. (24) can be easily shown using $\boldsymbol{\sigma}^x\boldsymbol{\sigma}^z\boldsymbol{\sigma}^x = -\boldsymbol{\sigma}^z$. Thus, by splitting the dispersive evolution of all N qubits into two equal halves and interspersing it with bit-flip operations on the qubits in S_M^c, we can effectively echo away the contribution of the latter to the total "magnetization" and implement the dispersive evolution $\boldsymbol{U}_{S_M}(t)$ of the qubits in S_M alone. Acting on an initial state of the form $|\alpha\rangle|\psi\rangle_N$, $\boldsymbol{U}_{S_M}(T = \pi/(2\chi))$ then encodes the subset-parity $\boldsymbol{Z}_{S_M} = \bigotimes_{i\in S_M}\boldsymbol{\sigma}_i^z$ onto the state of the cavity as explained above.

Physically, the initial unconditional cavity displacement and bit-flips can be implemented via fast microwave pulses (see supplemental material). Because of the dispersive interaction, the qubit transition frequency of the i-th qubit splits into a ladder of frequencies $\omega_{qi}^n = \omega_{qi}^0 + 2n\chi$, corresponding to different photon numbers in the cavity (Fig. 1 (c)). The latter are Poisson distributed and peaked around $\bar{n}$. Hence, to best approximate an unconditional rotation of the i-th qubit, the pulse must be centered at the frequency $\omega_{qi}^0 + 2\bar{n}\chi$ and have a frequency-width large compared with $2\sqrt{\bar{n}}\,\chi$. For $\bar{n} \geq 1/\pi$ the duration of such a π-pulse is thus $T_\pi \ll 1/(2\sqrt{\bar{n}}\chi) < T$. Similarly, the initial coherent state of the cavity $|\alpha\rangle$ can be prepared from the vacuum by driving the cavity at the frequency $\omega_c - \chi_A$ with a pulse of area α and a frequency-width large compared with $2N\chi$; the maximal frequency spread of a cavity dispersively coupled with strength χ to N qubits (Fig. 1 (b)). Again the duration T_d of this pulse is short since $T_d \ll 1/(2N\chi) < T$. The total duration of the encoding is thus dominated by the dispersive evolution time $T = \pi/(2\chi)$.

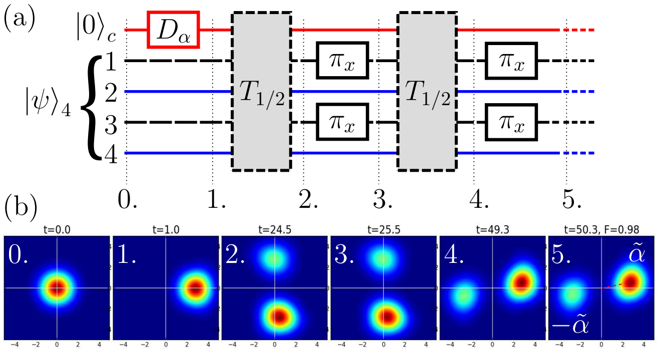

FIG. 2. (Color online) **(a)** Quantum circuit diagram for encoding the parity of qubits 2 and 4 (full (blue) lines). D_α represents the displacement operation, π_x a single-qubit π-pulse and $T_{1/2}$ a free dispersive evolution of duration $\pi/(4\chi)$. **(b)** Numerical simulation of the evolution of the Q-function of the cavity [25], with an initial qubit state $|\psi\rangle_4 = (|gge\rangle + |ggeg\rangle + |eeeg\rangle)/\sqrt{3}$. Dissipation from photon loss at a rate $\kappa/(2\pi) = 10\,$KHz and qubit decoherence with $T_1 = T_2 = 20\,\mu$s are included as well as a finite displacement and π-pulse duration of 1 ns. Other parameters are: $\alpha = 2$, $\chi/(2\pi) = 5\,$MHz and $K/(2\pi) = 80\,$KHz. The self-Kerr term leads to an additional phase rotation $\Delta\phi_{\rm nl} = 2K\bar{n}\Delta t$, where $\Delta t = 50.3\,$ns is the total duration of the encoding. Taking this rotation into account, we obtain a fidelity of $F = 98\%$ to the ideal target state $|\Psi\rangle_{\rm ideal} = |\tilde{\alpha}_2\rangle \boldsymbol{P}_{\{2,4\}}^{+}|\psi\rangle_4 + |-\tilde{\alpha}_2\rangle \boldsymbol{P}_{\{2,4\}}^{-}|\psi\rangle_4$.

Fig. 2 shows the quantum circuit diagram for the subset-parity encoding of $M = 2$ qubits out of $N = 4$ qubits along with the results of a numerical simulation with square cavity and qubit pulses of duration $T_\pi = T_d = 1\,$ns, dispersive shift $\chi/(2\pi) = 5\,$MHz and coherent state amplitude $\alpha = 2$. The initial four-qubit state is $|\psi\rangle_4 = (|gge\rangle + |ggeg\rangle + |eeeg\rangle)/\sqrt{3}$ and the simulation includes both dissipation from photon loss at a rate $\kappa/(2\pi) = 10\,$KHz and qubit decoherence with $T_1 = T_2 = 20\,\mu$s (see supplemental material). Furthermore we take into account a cavity nonlinearity of $K/(2\pi) = 80\,$KHz. Accounting for the phase rotation induced by the latter, and shortening the dispersive evolution times to compensate for the finite duration of the π-pulses, we find a fidelity (overlap with the ideal target state $|\Psi\rangle_{\rm ideal} = |\tilde{\alpha}_2\rangle \boldsymbol{P}_{\{2,4\}}^{+}|\psi\rangle_4 + |-\tilde{\alpha}_2\rangle \boldsymbol{P}_{\{2,4\}}^{-}|\psi\rangle_4$) of 98%. So far we have shown how to encode the parity of a weight $M \leq N$ $\boldsymbol{\sigma}^z$ Pauli operator $\boldsymbol{Z}_{S_M}$. By applying single-qubit rotations to individual qubits before and after the encoding one may in fact encode the parity of an arbitrary weight M Pauli operator $\boldsymbol{Q}_{S_M} = \bigotimes_{i\in S_M} \boldsymbol{\tau}_i$, with $\boldsymbol{\tau}_i \in \{\boldsymbol{\sigma}_i^x, \boldsymbol{\sigma}_i^y, \boldsymbol{\sigma}_i^z\}$. Next we explain how the encoded parity can be measured.

Parity readout. The encoded state is of the form $|\Psi\rangle_T = |\tilde{\alpha}_M\rangle \boldsymbol{P}_{S_M}^{+}|\psi\rangle_N + |-\tilde{\alpha}_M\rangle \boldsymbol{P}_{S_M}^{-}|\psi\rangle_N$, where in general $\boldsymbol{P}_{S_M}^{\pm} = (\mathbb{1} \pm \boldsymbol{Q}_{S_M})/2$ and $\tilde{\alpha}_M = (-i)^M e^{i\Delta\phi_{\rm nl}}\alpha$. The overlap between the two cavity states, $\langle\tilde{\alpha}_M|-\tilde{\alpha}_M\rangle = \exp(-2|\alpha|^2)$, is independent of K and M. For sufficiently large amplitude $|\alpha|$ of the initial displacement, these two states are distinguishable in principle and a measurement of the cavity state is equivalent to a multi-qubit parity measurement. A fast readout of the cavity state with $T_{\rm meas} \ll 1/\kappa$, may be achieved by lowering the Q-factor of the cavity containing the qubits ($\kappa \to \kappa' \gg \kappa$), as recently demonstrated [26]. This Q-switching adversely affects the lifetime of the qubits via the Purcell effect. However, the latter is expected to be weak as long as $\kappa' \ll \chi$. Alternatively, the cavity state can be mapped onto the ancilla qubit, which can subsequently be measured through standard homodyne measurement of the low-Q readout cavity. The mapping is achieved physically in three steps. First, the high-Q cavity field is displaced unconditionally by $\tilde{\alpha}_M$. To a good approximation, this maps the encoded state onto

$$\boldsymbol{D}_{\tilde{\alpha}_M}|\Psi\rangle_T = |2\tilde{\alpha}_M\rangle \boldsymbol{P}_{S_M}^{+}|\psi\rangle_N + |0\rangle \boldsymbol{P}_{S_M}^{-}|\psi\rangle_N\,. \tag{5}$$

The second step consists in performing a π-pulse on the ancilla qubit, which so far was in its ground state, conditioned on the cavity being in the vacuum state. As first proposed in [7] and demonstrated in [6], this can be achieved by applying a pulse centered on the bare ancilla qubit transition frequency, which is narrow in frequency compared with $8\bar{n}\chi_A$ (the additional factor of 4 is due to the twice as large amplitude of the cavity state in the first term on the rhs of Eq. (28)). Because $\chi_A \gg N\chi$, a pulse duration T_A can be chosen such that $1/(2\chi_A) \ll T_A \ll 1/(2N\chi)$. For $\bar{n} > 1/4$ the first inequality guarantees conditionality while the second one allows us to neglect the dispersive evolution during this operation. The state then becomes approximately

$$|2\tilde{\alpha}_M\rangle \Big(\boldsymbol{P}_{S_M}^{+}|\psi\rangle_N\Big)|g\rangle_A + |0\rangle \Big(\boldsymbol{P}_{S_M}^{-}|\psi\rangle_N\Big)|e\rangle_A. \tag{6}$$

In the third and final step, a displacement of $-2\tilde{\alpha}_M$ is performed on the cavity conditioned on the ancilla qubit being in the ground state. This is achieved with a pulse centered at frequency $\omega_c - \chi_A$, with a frequency-width small compared with $2\chi_A$ but large compared with $2N\chi$ (Fig. 1 (b)). Neglecting again the dispersive evolution during this step, the state finally becomes

$$|0\rangle \left[\left(\boldsymbol{P}^{+}_{S_M} |\psi\rangle_N \right) |g\rangle_A + \left(\boldsymbol{P}^{-}_{S_M} |\psi\rangle_N \right) |e\rangle_A \right]. \tag{7}$$

Note that the state (25) is now stationary with respect to the dispersive interaction, there being no photons in the cavity. Reading out the state of the ancilla qubit amounts to measuring $\boldsymbol{Q}_{S_M}$. After the measurement, the ancilla qubit may be reset to the ground state efficiently via the readout cavity [27].

Simulated time evolution. Apart from enabling a fast parity measurement, the ancilla qubit can also be used to simulate the "time evolution" $\exp[-i\theta \boldsymbol{Q}_{S_M}]$ under the action of an arbitrary Pauli operator $\boldsymbol{Q}_{S_M}$. This is useful e.g. for manipulating a logical qubit state encoded in a stabilizer subspace in which case $\boldsymbol{Q}_{S_M}$ is taken to be a logical qubit Pauli operator. Assuming that arbitrary rotations can be performed on the ancilla qubit in a time short compared with $1/(2N\chi)$, we start with Eq. (28) and perform a 2π-rotation of the ancilla around an axis $\vec{n} = (\sin(\varphi), 0, \cos(\varphi))$ with $\varphi = \arccos(1 - 2\theta/\pi)$, conditioned on the cavity being in the vacuum state. As a result, the odd-parity component of (28) acquires a phase 2θ (half the solid angle subtended by the ancilla state) and the state becomes

$$|2\tilde{\alpha}_M\rangle \boldsymbol{P}^{+}_{S_M} |\psi\rangle_N + e^{2i\theta} |0\rangle \boldsymbol{P}^{-}_{S_M} |\psi\rangle_N. \tag{8}$$

Note that in (31) we omitted the state of the ancilla qubit, since it starts and ends in the ground state and thus factors out. Finally the encoding is undone by applying the encoding protocol with α replaced by $-\tilde{\alpha}_M$. This disentangles the cavity and qubits and after unconditionally displacing the cavity back to the vacuum, taking into account an additional nonlinear phase acquired during the decoding, the N-qubit state becomes

$$\boldsymbol{P}^{+}_{S_M} |\psi\rangle_N + e^{2i\theta} \boldsymbol{P}^{-}_{S_M} |\psi\rangle_N = e^{i\theta} e^{-i\theta \boldsymbol{Q}_{S_M}} |\psi\rangle_N, \tag{9}$$

which up to an unimportant global phase factor, represents the action of the desired unitary.

Application. To test the feasibility of the above protocols, we simulated the preparation of a logical qubit state of the four-qubit erasure channel code [28]. The stabilizer generators of this code are $S = \{Z_1 Z_2, Z_3 Z_4, X_1 X_2 X_3 X_4\}$, where we have switched to the standard notation X_i and Z_i for the Pauli operators of qubit i. The code-space is spanned by the two $+1$ eigenstates of the stabilizers:

$$|\overline{0}\rangle = \frac{1}{2}(|gg\rangle + |ee\rangle)(|gg\rangle + |ee\rangle) \tag{10}$$

$$|\overline{1}\rangle = \frac{1}{2}(|gg\rangle - |ee\rangle)(|gg\rangle - |ee\rangle). \tag{11}$$

The logical qubit Pauli operators are $\overline{Z} = X_1 X_2 = X_3 X_4$ and $\overline{X} = Z_1 Z_3 = Z_2 Z_4 = Z_1 Z_4 = Z_2 Z_3$. Because of the redundancy of the logical operators, this code protects a logical qubit state $\alpha|\overline{0}\rangle + \beta|\overline{1}\rangle$ from the loss (i.e. arbitrary error) of a *known* qubit [28]. Here we prepare the logical qubit state $|\overline{\psi}\rangle = \exp[-i(\pi/8)\overline{X}]|\overline{0}\rangle$ as follows. (i) We start with the fully polarized four-qubit state $|gggg\rangle$, which is already a $+1$ eigenstate of the Z stabilizers. (ii) Using the encoding protocol, we measure the logical $\overline{Z}$ operator $X_1 X_2$. If we obtain -1, we apply Z_1. (iii) We measure the stabilizer $X_1 X_2 X_3 X_4$. If we obtain -1 we apply Z_3. In the absence of qubit-frequency tunability, Z_1 and Z_3 can be implemented, by combining two Hadamard rotations and a π-pulse [15]. (iv) We reset the cavity to the vacuum. These four steps prepare the logical state $|\overline{0}\rangle$. We next use the ancilla (with $\chi_A = 10N\chi$) to implement the rotation as described above with $\boldsymbol{Q}_{S_4} = \overline{X}$ and $\theta = \pi/8$. Fig. 3 shows the obtained fidelity to the ideal target state $\exp[-i(\pi/8)\overline{X}]|\overline{0}\rangle$ as a function of χ and K in units of $\kappa/(2\pi) = 10\,\mathrm{KHz}$ and for $T_1 = T_2 = 20\,\mu s$. The total duration T of the state preparation is shown on the upper x-axis in units of $1/\kappa$. Focusing on the line $K = 0$, when χ is small T is large and dominated by the dispersive evolutions and the fidelity is limited by a combination of qubit decoherence, photon loss and faulty conditional ancilla rotation. The fidelity then increases with increasing χ, which reduces the preparation time T and hence the effects of decoherence and improves the fidelity of the conditional ancilla rotation. It reaches a maximum in a regime where both conditional and unconditional operations can be performed with high fidelity. A further increase in χ degrades the unconditional cavity displacement and qubit rotations (a 1 ns pulse corresponds to a width of $\sim 160\,\mathrm{MHz}$) and the

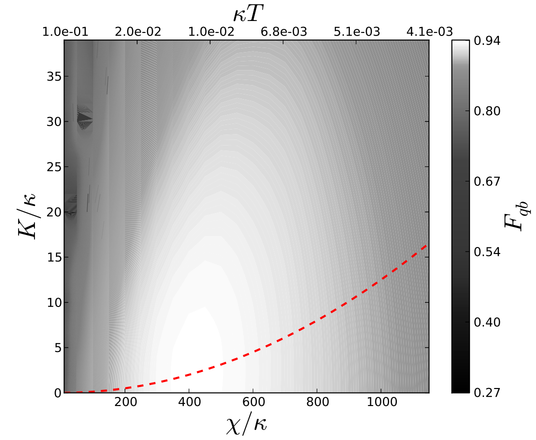

FIG. 3. (Color online) Fidelity of the prepared state to $\exp[-i(\pi/8)\overline{X}]|\overline{0}\rangle$. The (red) dashed curve represents the boundary of the inequality $K \geq \chi^2/(4\alpha_q)$ which relates the self-Kerr K with the dispersive shift χ and the single-qubit anharmonicity α_q [22]. Here $\alpha_q/(2\pi) = 200\,\mathrm{MHz}$.

fidelity drops. The cavity nonlinearity K and the dispersive shift χ are in fact not independent, but rather related via the single-qubit anharmonicity α_q, by the inequality $K \geq \chi^2/(4\alpha_q)$ [22], which is shown as a dashed (red) curve in Fig. 3 for $\alpha_q/(2\pi) = 200\,\mathrm{MHz}$.

Conclusion. We have proposed a protocol based on an echo technique to realize arbitrary stabilizer measurements with superconducting qubits in the ultra-strong dispersive regime. Numerical simulations, including decoherence and non-linear effects, show encouragingly high fidelities.

Acknowledgments. We thank L. Jiang, M. Mirrahimi and R. Schoelkopf for discussions. The simulations were coded in python using the QuTip library [29]. This work was supported by the Swiss NSF, the NSF (DMR-1004406) and the ARO (W911NF-09-1-0514).

---

[1] E. Lucero, R. Barends, Y. Chen, J. Kelly, M. Mariantoni, A. Megrant, P. OMalley, D. Sank, A. Vainsencher, J. Wenner, T. White, Y. Yin, A. N. Cleland, and J. M. Martinis, Nature Physics **8**, 719 (2012).

[2] M. D. Reed, L. DiCarlo, S. E. Nigg, L. Sun, L. Frunzio, S. M. Girvin, and R. J. Schoelkopf, Nature **482**, 382 (2012).

[3] D. Gottesman, *Stabilizer Codes and Quantum Error Correction*, Ph.D. thesis, Caltech (1997).

[4] H. Paik, D. I. Schuster, L. S. Bishop, G. Kirchmair, G. Catelani, A. P. Sears, B. R. Johnson, M. J. Reagor, L. Frunzio, L. I. Glazman, S. M. Girvin, M. H. Devoret, and R. J. Schoelkopf, Phys. Rev. Lett. **107**, 240501 (2011).

[5] C. Rigetti, J. M. Gambetta, S. Poletto, B. L. T. Plourde, J. M. Chow, A. D. Córcoles, J. A. Smolin, S. T. Merkel, J. R. Rozen, G. A. Keefe, M. B. Rothwell, M. B. Ketchen, and M. Steffen, Phys. Rev. B **86**, 100506 (2012).

[6] G. Kirchmair, B. Vlastakis, Z. Leghtas, S. E. Nigg, H. Paik, E. Ginossar, M. Mirrahimi, L. Frunzio, S. M. Girvin, and R. J. Schoelkopf, (2012), arXiv:1211.2228 [quant-ph].

[7] Z. Leghtas, G. Kirchmair, B. Vlastakis, M. Devoret, R. Schoelkopf, and M. Mirrahimi, (2012), arXiv:1205.2401 [quant-ph].

[8] Z. Leghtas, G. Kirchmair, B. Vlastakis, R. Schoelkopf, M. Devoret, and M. Mirrahimi, (2012), arXiv:1207.0679 [quant-ph].

[9] K. Lalumière, J. M. Gambetta, and A. Blais, Phys. Rev. A **81**, 040301 (2010).

[10] D. P. DiVincenzo and S. Firat, (2012), arXiv:1205.1910 [quant-ph].

[11] R. Raussendorf and H. J. Briegel, Phys. Rev. Lett. **86**, 5188 (2001); R. Raussendorf, D. E. Browne, and H. J. Briegel, Phys. Rev. A **68**, 022312 (2003).

[12] A. Kitaev, Annals of Physics **303**, 2 (2003).

[13] A. G. Fowler, M. Mariantoni, J. M. Martinis, and A. N. Cleland, Phys. Rev. A **86**, 032324 (2012); J. Ghosh, A. G. Fowler, and M. R. Geller, arXiv:1210.5799 [quant-ph].

[14] J. T. Barreiro, M. Müller, P. Schindler, D. Nigg, T. Monz, M. Chwalla, M. Hennrich, C. F. Roos, P. Zoller, and R. Blatt, Nature **470**, 486 (2011); M. Müller, K. Hammerer, Y. L. Zhou, C. F. Roos, and P. Zoller, New. J. Phys. **13**, 085007 (2011).

[15] A. Blais, R.-S. Huang, A. Wallraff, S. M. Girvin, and R. J. Schoelkopf, Phys. Rev. A **69**, 062320 (2004).

[16] D. I. Schuster, A. A. Houck, J. A. Schreier, A. Wallraff, J. M. Gambetta, A. Blais, L. Frunzio1, J. Majer, B. Johnson, M. H. Devoret, S. M. Girvin, and R. J. Schoelkopf, Nature **445**, 515 (2007).

[17] J. Koch, T. M. Yu, J. Gambetta, A. A. Houck, D. I. Schuster, J. Majer, A. Blais, M. H. Devoret, S. M. Girvin, and R. J. Schoelkopf, Phys. Rev. A **76**, 042319 (2007).

[18] M. Lenander, H. Wang, R. C. Bialczak, E. Lucero, M. Mariantoni, M. Neeley, A. D. O'Connell, D. Sank, M. Weides, J. Wenner, T. Yamamoto, Y. Yin, J. Zhao, A. N. Cleland, and J. M. Martinis, Phys. Rev. B **84**, 024501 (2011).

[19] G. Catelani, R. J. Schoelkopf, M. H. Devoret, and L. I. Glazman, Phys. Rev. B **84**, 064517 (2011).

[20] G. Catelani, S. E. Nigg, S. M. Girvin, R. J. Schoelkopf, and L. I. Glazman, Phys. Rev. B **86**, 184514 (2012).

[21] L. DiCarlo, J. M. Chow, J. M. Gambetta, L. S. Bishop, B. R. Johnson, D. I. Schuster, J. Majer, A. Blais, L. Frunzio, S. M. Girvin, and R. J. Schoelkopf, Nature **460**, 240 (2009).

[22] S. E. Nigg, H. Paik, B. Vlastakis, G. Kirchmair, S. Shankar, L. Frunzio, M. H. Devoret, R. J. Schoelkopf, and S. M. Girvin, Phys. Rev. Lett. **108**, 240502 (2012).

[23] J. Bourassa, F. Beaudoin, J. M. Gambetta, and A. Blais, Phys. Rev. A **86**, 013814 (2012).

[24] Qubit-state-dependent corrections to the self-Kerr are of order $\hat{\varphi}^6$ in an expansion of the Josephson potential $E_J \cos(\hat{\varphi})$ and are smaller by a factor $\sim \sqrt{E_C/E_J}$.

[25] D. F. Walls and G. J. Milburn, *Quantum optics*, 2nd ed. (Springer, 2008).

[26] Y. Yin, Y. Chen, D. Sank, P. J. J. O'Malley, T. C. White, R. Barends, J. Kelly, E. Lucero, M. Mariantoni, A. Megrant, C. Neill, A. Vainsencher, J. Wenner, A. N. Korotkov, A. N. Cleland, and J. M. Martinis, (2012), arXiv:1208.2950 [cond-mat].

[27] K. Geerlings, Z. Leghtas, I. M. Pop, S. Shankar, L. Frunzio, R. J. Schoelkopf, M. Mirrahimi, and M. H. Devoret, (2012), arXiv:1211.0491 [cond-mat.mes-hall].

[28] M. Grassl, T. Beth, and T. Pellizzari, Phys. Rev. A **56**, 33 (1997).

[29] J. Johansson, P. Nation, and F. Nori, Computer Physics Communications **183**, 1760 (2012).

[30] A derivation which goes beyond this simple dipole approximation to include the exact linear normal modes is given in [22, 23].

[31] We also neglect multi-photon processes.

[32] M. Boissonneault, J. M. Gambetta, and A. Blais, Phys. Rev. Lett. **105**, 100504 (2010).

[33] H.-P. Breuer and F. Petruccione, *The theory of open quantum systems* (Oxford Univ. Press, 2007).

Supplemental Material for
“Stabilizer quantum error correction toolbox for superconducting qubits”

Simon E. Nigg and S. M. Girvin
Departments of Physics, Yale University, New Haven, CT 06520, USA
(Dated: December 21, 2012)

In these notes, we derive the effective Hamiltonian of Eq. (1) in the main text. We calculate finite pulse-width effects for the unconditional displacement and single-qubit rotations and discuss the constraints imposed on the drive and system spectrum. We describe a modification of the parity measurement protocol for stabilizer pumping. We briefly discuss our treatment of decoherence and present the state tomography of the encoded logical qubit state. Finally we conclude with a discussion of possible applications and extensions.

DERIVATION OF THE EFFECTIVE MODEL OF EQ. (1)

In terms of its two conjugate variables $\boldsymbol{\varphi}$ and $\boldsymbol{n}$, which represent the superconducting phase difference and the number of Cooper pairs transferred across the Josephson junction (JJ), a transmon qubit is conventionally described by the Hamiltonian [17]

$$H = 4E_C(\boldsymbol{n}-n_g)^2 + E_J(1-\cos(\boldsymbol{\varphi})) = 4E_C(\boldsymbol{n}-n_g)^2 + \frac{E_J}{2}\boldsymbol{\varphi}^2 + V_{\rm nl}(\boldsymbol{\varphi})\,. \tag{12}$$

In the second equality we have explicitly separated the harmonic and anharmonic parts of the Josephson potential $E_J(1-\cos(\boldsymbol{\varphi})) = \boldsymbol{\varphi}^2 E_J/2 + V_{\rm nl}(\boldsymbol{\varphi})$. For $E_J \gg E_C$, the “phase particle” essentially undergoes quasi-harmonic oscillations around a local minimum of the cosine potential, with rare 2π quantum phase-slip events, which lead to a weak (exponentially suppressed in E_J/E_C) dependence of the energy levels on the offset charge n_g [17]. In the following we will neglect the latter and set $n_g = 0$. It is convenient to diagonalize the harmonic part by introducing the bare mode operator $\boldsymbol{a}_0 = \sqrt{E_J/(2\hbar\omega_0)}\,\boldsymbol{\varphi} + 2i\sqrt{E_C/(\hbar\omega_0)}\,\boldsymbol{n}$ and frequency $\hbar\omega_0 = \sqrt{8E_JE_C}$. Then expanding the non-linear potential to leading order ($\boldsymbol{\varphi}^4$) one obtains

$$H = \hbar\omega_0(\boldsymbol{a}_0^\dagger\boldsymbol{a}_0 + 1/2) - \frac{E_C}{12}(\boldsymbol{a}_0 + \boldsymbol{a}_0^\dagger)^4 + \mathcal{O}(\boldsymbol{\varphi}^6) \tag{13}$$

Note that the coefficient of a given term in the expansion is smaller than the previous one by a factor $\sim \sqrt{E_C/E_J}$. We are primarily interested in low-lying energy levels, for which the wavefunctions are localized in phase i.e. $\sqrt{\langle\boldsymbol{\varphi}^2\rangle} \ll \pi$. Hence we consider here only the leading order φ^4 non-linearity.

The coupling of a transmon with the electromagnetic field of a resonator is typically described in the dipole approximation [30] by a term $\sim \boldsymbol{n}\cdot\boldsymbol{E}$ where $\boldsymbol{E} = \sum_k i\epsilon_k(\boldsymbol{b}_k - \boldsymbol{b}_k^\dagger)$ is the quantized electric field of the (multi-mode) resonator written in terms of its eigenmodes $\boldsymbol{b}_k$. In a straightforward generalization of the above, the Hamiltonian of $N_{\rm qb}$ transmons coupled to multiple harmonic modes can be written in the general form (suppressing from now on the zero-point energies)

$$H = \sum_{i=1}^{N_{\rm qb}} \hbar\omega_i^{\rm qb}\boldsymbol{a}_i^\dagger\boldsymbol{a}_i + \sum_j \hbar\omega_j^{\rm c}\boldsymbol{b}_j^\dagger\boldsymbol{b}_j + \sum_{ij} g_{ij}(\boldsymbol{a}_i - \boldsymbol{a}_i^\dagger)(\boldsymbol{b}_j - \boldsymbol{b}_j^\dagger) + \sum_{i=1}^{N_{\rm qb}} V_{\rm nl}^{(i)}(\boldsymbol{\varphi}_i) \quad \text{with} \quad g_{ij} = \frac{\epsilon_j}{2}\sqrt{\frac{\hbar\omega_i^{\rm qb}}{E_C^{(i)}}} \tag{14}$$

Here $V_{\rm nl}^{(i)}(\boldsymbol{\varphi}_i) = E_J^{(i)}[(1-\cos(\boldsymbol{\varphi}_i)) - {\boldsymbol{\varphi}_i}^2/2]$. As before, it is convenient to diagonalize the harmonic part. As shown in [22], this diagonalization can be achieved from the knowledge of the $N_{\rm qb}\times N_{\rm qb}$ impedance matrix $\boldsymbol{Z}$ of the corresponding linearized circuit with each one of the $N_{\rm qb}$ JJs representing a port. Denoting the normal modes by $\boldsymbol{c}_p$ and their frequencies by ω_p, one obtains explicitly

$$\boldsymbol{\varphi}_i^{(k)} = \phi_0^{-1}\sum_{p=1}^{M}\frac{\boldsymbol{Z}_{ik}(\omega_p)}{\boldsymbol{Z}_{kk}(\omega_p)}\sqrt{\frac{\hbar}{2}\mathcal{Z}_{kp}^{\rm eff}}\,(\boldsymbol{c}_p + \boldsymbol{c}_p^\dagger) \quad \text{with} \quad \mathcal{Z}_{kp}^{\rm eff} = \frac{2}{\omega_p {\rm Im}[\partial_\omega Y_k(\omega_p)]} \tag{15}$$

Here $\phi_0 = \hbar/(2e)$ is the reduced flux quantum and we have introduced the admittance at port k defined as $Y_k = 1/\boldsymbol{Z}_{kk}$. The choice of the port k is arbitrary and reflects a particular basis choice. The total number of modes is denoted by

M. The mode frequencies ω_p are given by the zeros of the imaginary part of the admittance, i.e. $\mathrm{Im}Y_k(\omega_p) = 0$ (note that in the dissipationless case, the elements of $\boldsymbol{Z}$ are purely imaginary).

Keeping the leading order φ^4 non-linearity and normal-ordering the latter, the Hamiltonian of the system then takes the form

$$\begin{aligned} H_4 = &\sum_p \omega_p \boldsymbol{c}_p^\dagger \boldsymbol{c}_p - \sum_{pp'} \gamma_{pp'} \left(2\boldsymbol{c}_p^\dagger \boldsymbol{c}_{p'} + \boldsymbol{c}_p^\dagger \boldsymbol{c}_{p'}^\dagger + \boldsymbol{c}_p \boldsymbol{c}_{p'} \right) \\ &- \sum_{pp'qq'} \beta_{pp'qq'} \left(6\boldsymbol{c}_p^\dagger \boldsymbol{c}_{p'}^\dagger \boldsymbol{c}_q \boldsymbol{c}_{q'} + 4\boldsymbol{c}_p^\dagger \boldsymbol{c}_{p'}^\dagger \boldsymbol{c}_q^\dagger \boldsymbol{c}_{q'} + 4\boldsymbol{c}_p^\dagger \boldsymbol{c}_{p'} \boldsymbol{c}_q \boldsymbol{c}_{q'} + \boldsymbol{c}_p \boldsymbol{c}_{p'} \boldsymbol{c}_q \boldsymbol{c}_{q'} + \boldsymbol{c}_p^\dagger \boldsymbol{c}_{p'}^\dagger \boldsymbol{c}_q^\dagger \boldsymbol{c}_{q'}^\dagger \right), \end{aligned} \tag{16}$$

with

$$\beta_{pp'qq'} = R_0^{-2} \sqrt{\mathcal{Z}_{kp}^{\mathrm{eff}} \mathcal{Z}_{kp'}^{\mathrm{eff}} \mathcal{Z}_{kq}^{\mathrm{eff}} \mathcal{Z}_{kq'}^{\mathrm{eff}}} \sum_{i=1}^{N_{\mathrm{qb}}} \frac{E_J^{(i)}}{6} \frac{\boldsymbol{Z}_{ik}(\omega_p)}{\boldsymbol{Z}_{kk}(\omega_p)} \frac{\boldsymbol{Z}_{ik}(\omega_{p'})}{\boldsymbol{Z}_{kk}(\omega_{p'})} \frac{\boldsymbol{Z}_{ik}(\omega_q)}{\boldsymbol{Z}_{kk}(\omega_q)} \frac{\boldsymbol{Z}_{ik}(\omega_{q'})}{\boldsymbol{Z}_{kk}(\omega_{q'})} \tag{17}$$

where $R_0 = \hbar/e^2$ and $\gamma_{pp'} = 6\sum_q \beta_{qqpp'}$. Eqs. (16) and (17) together with a model for the impedance matrix, allow one to design the circuit Hamiltonian [22, 23]. Importantly, the above derivation provides the functional dependence among the parameters ω_p, $\gamma_{p'}$ and $\beta_{pp'qq'}$. By applying a generalized RWA in the dispersive limit of large detuning between the modes [31], we may neglect rapidly-rotating and non-diagonal terms and thus consider the simplified form

$$H_{\mathrm{eff}} = \sum_p \omega_p' \boldsymbol{c}_p^\dagger \boldsymbol{c}_p + \frac{1}{2} \sum_{pq} \chi_{pq} \boldsymbol{c}_p^\dagger \boldsymbol{c}_q^\dagger \boldsymbol{c}_q \boldsymbol{c}_p \tag{18}$$

where we have defined $\chi_{pq} = -24\beta_{pqqp}$ for $q \neq p$ and $\chi_{pp} = -12\beta_{pppp}$. The frequencies have been renormalized as $\omega_p' = \omega_p - 2\gamma_{pp}$. The second term on the rhs of (18) describes self-Kerr (χ_{pp}) and cross-Kerr (χ_{qp} with $q \neq p$) interactions between the modes. From the Cauchy-Schwarz inequality and Eq. (17), it can be shown that $\chi_{qp}^2 \leq 4\chi_{qq}\chi_{pp}$; equality holding in the single-qubit case. In the dispersive regime of interest here, the hybridization of qubit and cavity modes is small and one can unambiguously identify the qubit-like modes as those with the strongest anharmonicities. Assuming the latter are much larger than the linewidth and as long as the drive frequencies used are different from transitions between the first and second excited states, the qubit Hilbert space can be truncated to the lowest two levels. From (18) we then obtain, denoting the cavity modes with $\boldsymbol{a}_i$ and suppressing constant terms

$$H_0 = \sum_{i=1}^{N_{\mathrm{qb}}} \frac{\omega_i^{\mathrm{qb}}}{2} \boldsymbol{\sigma}_i^z + \sum_j \omega_j^{\mathrm{c}} \boldsymbol{a}_j^\dagger \boldsymbol{a}_j + \sum_{i=1}^{N_{\mathrm{qb}}} \sum_j \chi_{ij} \boldsymbol{\sigma}_i^z \boldsymbol{a}_j^\dagger \boldsymbol{a}_j - \sum_i K_i \boldsymbol{a}_i^\dagger \boldsymbol{a}_i^\dagger \boldsymbol{a}_i \boldsymbol{a}_i\,, \tag{19}$$

where $K_i \equiv \chi_{ii}$ and we have kept only the dispersive and qubit-cavity cross-Kerr shifts. We note that in addition to these interaction terms there exist in general also qubit-qubit ($\sim \boldsymbol{\sigma}_i^z \boldsymbol{\sigma}_j^z$, $i \neq j$) and cavity-cavity ($\sim \boldsymbol{a}_i^\dagger \boldsymbol{a}_i \boldsymbol{a}_j^\dagger \boldsymbol{a}_j$, $i \neq j$) cross-Kerr shifts. However in the regime of interest here, the coefficients of these terms are small and will consequently be neglected.

A qubit-induced cavity non-linearity has previously been derived within the dispersive approximation of a multi-level generalization of the Tavis-Cummings model [32]. In addition to the qubit independent term discussed here, such a treatment also yields qubit dependent non-linearities. In our derivation, qubit dependent self-Kerr terms appear only at order φ^6 and higher and are parametrically small for large ratios E_J/E_C.

We can now apply (19) to our system depicted in Fig. 1 of the main text. From the above derivation, we see that in principle all qubits (N active qubits and 1 ancilla qubit) couple to multiple modes of both cavities. However, in the weakly coupled dispersive limit for the readout cavity and appropriately chosen parameters, we may neglect the coupling of the active qubits with the readout (low-Q) cavity mode and higher modes of the active (high-Q) cavity. Similarly the ancilla approximately only couples to a single mode in each cavity. Choosing the dispersive shifts of the active qubits to be all equal to χ and denoting the dispersive shift of the ancilla with the active cavity mode $\boldsymbol{a}$ by $\chi_A \gg N\chi$ and with the readout cavity mode $\boldsymbol{b}$ by χ_A' we obtain

$$H_0 = \sum_{i=1}^{N} \frac{\omega_i^{\mathrm{qb}}}{2} \boldsymbol{\sigma}_i^z + \omega_{\mathrm{c}} \boldsymbol{a}^\dagger \boldsymbol{a} + \chi \sum_{i=1}^{N} \boldsymbol{\sigma}_i^z \boldsymbol{a}^\dagger \boldsymbol{a} + \chi_A \boldsymbol{\sigma}_z^A \boldsymbol{a}^\dagger \boldsymbol{a} - K \boldsymbol{a}^\dagger \boldsymbol{a}^\dagger \boldsymbol{a} \boldsymbol{a} + H_{\mathrm{readout}}\,, \tag{20}$$

with $H_{\mathrm{readout}} = \omega_{\mathrm{c}}' \boldsymbol{b}^\dagger \boldsymbol{b} + \chi_A' \sigma_z^A \boldsymbol{b}^\dagger \boldsymbol{b} - K' \boldsymbol{b}^\dagger \boldsymbol{b}^\dagger \boldsymbol{b}\boldsymbol{b}$. Finally, moving to a frame rotating with qubits and cavity by the unitary transformation $\boldsymbol{U}(t) = \exp\left[-it\left(\sum_i (\omega_i^{\mathrm{qb}}/2)\boldsymbol{\sigma}_i^z + (\omega_c - \chi_A)\boldsymbol{a}^\dagger\boldsymbol{a}\right)\right]$ yields Eq. (1) of the main text:

$$H_0 = \chi \sum_{i=1}^{N} \boldsymbol{\sigma}_i^z \boldsymbol{a}^\dagger \boldsymbol{a} - K \boldsymbol{a}^\dagger \boldsymbol{a}^\dagger \boldsymbol{a}\boldsymbol{a}\,. \tag{21}$$

This model is a valid when the ancilla qubit and readout cavity remain in their ground state, in which case $H_{\mathrm{readout}} = 0$.

FINITE PULSE-WIDTH EFFECTS ON UNCONDITIONAL OPERATIONS

Having motivated the form of our Hamiltonian (21) [Eq. (1) of the main text], we next use it to investigate the effects due to finite pulse-width when driving the system with realistic pulses. To distinguish these effects from the nonlinear effects we here set $K = 0$. In the following discussion, we concentrate on the unconditional operations necessary for the parity encoding protocol and neglect the ancilla qubit and readout cavity. We further assume independent drives for the qubits and the cavity mode. For the latter to be a valid approximation, the qubits need to be sufficiently detuned from each other and from the cavity. In the rotating frame of Eq. (21), a cavity drive at frequency ω_d is then described by

$$H_d^{\mathrm{c}}(t) = \varepsilon_0(t)(e^{it(\omega_{\mathrm{c}} - \chi_A - \omega_d)}\boldsymbol{a}^\dagger + h.c.). \tag{22}$$

In the same rotating frame, a simultaneous drive of the qubits in a set $S \in S_N = \{1, \ldots, N\}$ at frequencies ω_i^d for $i \in S$, is described by a term

$$H_d^{\mathrm{qb}}(t) = \sum_{i \in S} \frac{\Omega_i(t)}{2}(\boldsymbol{\sigma}_i^+ e^{it(\omega_i^{\mathrm{qb}} - \omega_i^d)} + h.c.). \tag{23}$$

Unconditional displacement

At the start of the encoding, we need to be able to displace the cavity from the vacuum into a coherent state with amplitude α independently of the state of the qubits. We choose $\omega_d = \omega_c - \chi_A$ and consider the Hamiltonian

$$H(t) = \chi\left(\sum_{i=1}^{N} \sigma_i^z\right)\boldsymbol{a}^\dagger\boldsymbol{a} + \varepsilon_0(t)(\boldsymbol{a} + \boldsymbol{a}^\dagger). \tag{24}$$

Let us denote the computational basis states of N qubits by $|i_1, \ldots, i_N\rangle$, with $\boldsymbol{\sigma}_j^z |i_j\rangle = i_j |i_j\rangle$ and $i_j \in \{-1, 1\}$. Under the action of the Hamiltonian (24), the initial product state $|0\rangle_c |\psi\rangle_N$ with $|\psi\rangle_N = \sum_{i_1,\ldots,i_N} c_{i_1,\ldots,i_N} |i_1, \ldots, i_N\rangle$ evolves into

$$|\psi(t)\rangle = \sum_{i_1,\ldots,i_N} c_{i_1,\ldots,i_N} \left| -i \int_0^t d\tau \varepsilon_0(\tau) e^{i\chi(\tau - t)A_{i_1,\ldots,i_N}} \right\rangle |i_1, \ldots, i_N\rangle, \tag{25}$$

where $A_{i_1,\ldots,i_N} = \sum_{j=1}^{N} i_j$.

For simplicity, we consider a square pulse with envelope $\varepsilon_0(t) = \epsilon_0 \theta(T - t)$. The amplitude of the coherent state associated with the qubit component $|i_1, \ldots, i_N\rangle$ at time T becomes

$$\alpha_T = -i\epsilon_0 T e^{-\frac{i\chi A_{i_1,\ldots,i_N} T}{2}} \operatorname{sinc}\left(\chi A_{i_1,\ldots,i_N} T/2\right), \tag{26}$$

where $\operatorname{sinc}(x) = \sin(x)/x$. Thus there is both a qubit-state dependent rotation and a suppression of the amplitude of the coherent state. Since $-N \leq A_{i_1,\ldots,i_N} \leq N$, if $N\chi T \ll 1$, we can expand and obtain

$$\alpha_T = -i\epsilon_0 T - \epsilon_0 T^2 \chi \frac{A_{i_1,\ldots,i_N}}{2} + \mathcal{O}((N\chi T)^2). \tag{27}$$

Thus the first-order correction to the displacement of the cavity state is a qubit-state dependent rotation. The change in amplitude is second order in $N\chi T$. This has important consequences for the encoding protocol, since it allows for a partial compensation of the finite pulse-length effect of the displacement simply by shortening the duration of the subsequent free evolution part. Retaining only the leading order term, the state in (25) factorizes and we have

$$|\psi(T)\rangle \approx |-i\epsilon_0 T\rangle|\psi\rangle_N. \tag{28}$$

which corresponds to a cavity displaced by $\alpha = -i\epsilon_0 T$, while the qubits were left unchanged. In terms of the drive strength and final coherent state amplitude, this is valid when $|\alpha| \ll \epsilon_0/(N\chi)$. Because $-N \leq A_{i_1,\ldots,i_N} \leq N$, the maximum amplitude difference is given to first order by $\epsilon_0 T^2 N\chi = |\alpha|N\chi T$. We may then define a fidelity of the displacement operation as the absolute value of the overlap between an ideally displaced coherent state and a state with maximal phase difference. To leading order, this is found to be

$$F \approx \exp\left[-\frac{1}{8}\left(|\alpha|NT\chi\right)^2\right]. \tag{29}$$

Thus we see that to achieve high fidelity, the average number of photons in the cavity $\bar{n} = |\alpha|^2$ should satisfy $\sqrt{\bar{n}}N\chi T \ll 8$. Fig. 4 shows the numerically computed fidelity to the target displaced state obtained from the initial state $|0\rangle_c|gggg\rangle$ as a function of the square pulse duration T. For this simulation we took $\chi/(2\pi) = 10\,\text{MHz}$, $\alpha = 2.5$.

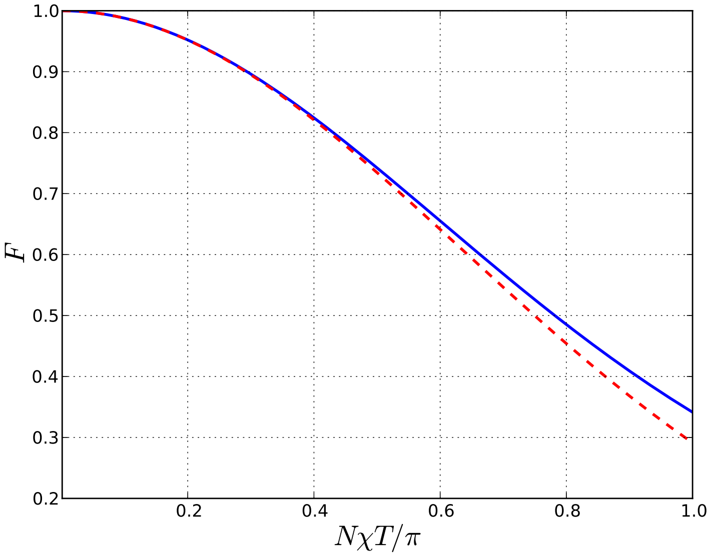

FIG. 4. Fidelity of un-conditional displacement for the initial state $|0\rangle_c|gggg\rangle_{N=4}$ as a function of square pulse duration T. The dashed (red) curve shows $F = \exp[-(|\alpha|N\chi T)^2/8]$. We took a dispersive shift $\chi/(2\pi) = 10\,\text{MHz}$, and a cavity displacement $\alpha = 2.5$.

Unconditional qubit selective π-pulses

In order to perform subset-selective parity measurements, one needs to perform unconditional π-pulses on subsets of qubits as explained in the main text. The qubits can be driven simultaneously by using a polychromatic drive. Following the discussion in the main text we choose the drive frequencies to be $\omega_i^d = \omega_i^{\text{qb}} + 2\bar{n}\chi$ and thus consider the following Hamiltonian in the rotating frame

$$H(t) = \chi\left(\sum_{i=1}^{N}\sigma_i^z\right)\boldsymbol{a}^\dagger\boldsymbol{a} + \sum_{j\in S_M^c}\frac{\Omega_j(t)}{2}\left(e^{2i\bar{n}\chi t}\boldsymbol{\sigma}_j^- + h.c.\right). \tag{30}$$

Note that here we have neglected the off-resonant driving of the qubits in S_M. In order for this to be valid, we must require the frequency detuning between any two qubits to be large compared with $2\sqrt{\bar{n}}\chi$. Moving to a frame rotating with the qubits in S_M^c at frequency $\bar{n}\chi$, we can write the Hamiltonian as (we use the same symbol H to denote the Hamiltonian in the new frame)

$$H = \chi \left(\sum_{j \in S_M} \boldsymbol{\sigma}_j^z \right) \boldsymbol{a}^\dagger \boldsymbol{a} + \chi \left(\sum_{j \in S_M^c} \boldsymbol{\sigma}_j^z \right) (\boldsymbol{a}^\dagger \boldsymbol{a} - \bar{n}) + \sum_{j \in S_M^c} \frac{\Omega_j(t)}{2} \boldsymbol{\sigma}_j^x \, . \tag{31}$$

Clearly the first term on the rhs commutes with the remaining terms and leads to a "free" evolution of the qubits in S_M and of the cavity given by $\boldsymbol{U}_{S_M}(t) = \exp(-it\chi \boldsymbol{a}^\dagger \boldsymbol{a} \sum_{i \in S_M} \boldsymbol{\sigma}_i^z)$. The action of the last two terms on each qubit in S_M^c is described by a single qubit Hamiltonian of the form

$$H_1 = \chi \boldsymbol{\sigma}^z (\boldsymbol{a}^\dagger \boldsymbol{a} - \bar{n}) + \frac{\Omega(t)}{2} \boldsymbol{\sigma}^x . \tag{32}$$

Defining $\beta(t) = \int_0^t \frac{\Omega(\tau)}{2} d\tau$, the associated evolution operator is

$$\boldsymbol{U}_1(t) = e^{-i\beta(t)\boldsymbol{\sigma}^x} e^{-i\chi(\boldsymbol{a}^\dagger \boldsymbol{a} - \bar{n}) \int_0^t d\tau \left\{ \boldsymbol{\sigma}^z [\cos^2(\beta(\tau)) - \sin^2(\beta(\tau))] + 2\boldsymbol{\sigma}^y \sin(\beta(\tau)) \cos(\beta(\tau)) \right\}} . \tag{33}$$

For $\chi = 0$ this reduces to a simple $\boldsymbol{\sigma}^x$ rotation, the angle of which is determined by the integral of the pulse envelope. The total evolution operator, including the contribution from the first term on the rhs of (31), is then

$$\boldsymbol{U}(t) = \boldsymbol{U}_{S_M}(t) e^{-i\beta(t) \sum_{j \in S_M^c} \boldsymbol{\sigma}_j^x} e^{-i\chi(\boldsymbol{a}^\dagger \boldsymbol{a} - \bar{n}) \sum_{j \in S_M^c} \int_0^t d\tau \left\{ \boldsymbol{\sigma}_j^z [\cos^2(\beta(\tau)) - \sin^2(\beta(\tau))] + 2\boldsymbol{\sigma}_j^y \sin(\beta(\tau)) \cos(\beta(\tau)) \right\}} . \tag{34}$$

For a square pulse envelope $\Omega(t) = \Omega_0 \theta(T - t)$ with $T = \pi/\Omega_0$ such that $\beta(T) = \pi/2$ it is easy to show that

$$\boldsymbol{U}(T) = \boldsymbol{U}_{S_M} \left(\frac{\pi}{\Omega_0} \right) e^{-\frac{i\pi}{2} \sum_{j \in S_M^c} \boldsymbol{\sigma}_j^x} e^{-\frac{2i\chi}{\Omega_0} (\boldsymbol{a}^\dagger \boldsymbol{a} - \bar{n}) \sum_{j \in S_M^c} \boldsymbol{\sigma}_j^y} . \tag{35}$$

We are interested in the action of this operator on a coherent state or superposition of coherent states, for which the photon number is Poisson distributed around $\bar{n}$ with variance equal to $\bar{n}$. Hence if $2\sqrt{\bar{n}}\chi \ll \Omega_0$, we have

$$\boldsymbol{U}(T) \approx \boldsymbol{U}_{S_M}(T) \left[(-i)^M \prod_{j \in S_M} \boldsymbol{\sigma}_j^x + \mathcal{O}\left(\frac{2\sqrt{\bar{n}}\chi T}{\pi} \right) \right] . \tag{36}$$

If furthermore, we require that $2\chi M \pi \ll \Omega_0$, then $\boldsymbol{U}_{S_M} \approx \mathbb{1} + \mathcal{O}(2\chi M T)$ so that

$$\boldsymbol{U}(T) \approx (-i)^M \prod_{j \in S_M} \boldsymbol{\sigma}_j^x + \mathcal{O}\left(\frac{2\sqrt{\bar{n}}\chi T}{\pi}, 2\chi M T \right) . \tag{37}$$

Fig. 5 shows the fidelity as a function of the square pulse duration T, of an unconditional two-qubit π rotation acting on an initial state $|\alpha\rangle_c |\psi\rangle_4$ with $|\psi\rangle_4 = \sqrt{1/3}(|eegg\rangle + |eggg\rangle - |egge\rangle)$, $\alpha = 2.5$ and for $\chi/(2\pi) = 10\,\text{MHz}$.

STABILIZER PUMPING

In the main text we show how to measure a stabilizer by first encoding its eigenvalues onto the cavity state and then reading out the latter either directly or via the ancilla qubit and the readout cavity. Alternatively one can also implement conditional jump operators of the form $\boldsymbol{\sigma}_i^x \boldsymbol{P}_{S_M}^-$ where $\boldsymbol{P}_{S_M}^\pm = (\mathbb{1} \pm \boldsymbol{Z}_{S_M})/2$ with $\boldsymbol{Z}_{S_M} = \prod_{i \in S_M} \boldsymbol{\sigma}_i^z$ and $i \in S_M$. Such operators can be used to digitally simulate an artificial bath that pumps the system onto the stabilizer subspace as first proposed for trapped ions in [14]. The dissipative evolution under the action of such jump operators can be implemented with the protocol shown in Fig. 6. As for a parity measurement, one first encodes the eigenvalues of the parity operator onto the cavity state and applies and unconditional displacement to obtain the state (see Eq. (5) of the main text)

$$|\Psi\rangle = |2\tilde{\alpha}_N\rangle \boldsymbol{P}_{S_M}^+ |\psi\rangle_N + |0\rangle \boldsymbol{P}_{S_M}^- |\psi\rangle_N \, . \tag{38}$$

Instead of mapping the cavity state onto an ancilla as in the measurement protocol, one then applies a rotation by an angle θ around x of qubit $i \in S_M$ *conditioned* on the cavity being in the vacuum state. Note that this does not require an ancilla qubit. Because $\{\sigma_i^x, Z_{S_M}\}_+ = 0$ for $i \in S_M$, the state becomes

$$\boldsymbol{P}_{S_M}^+ \left(|\psi\rangle_N |2\alpha\rangle_c + i \sin(\theta/2) \sigma_i^x |\psi\rangle_N |0\rangle_c \right) + \cos(\theta/2) \boldsymbol{P}_{S_M}^- |\psi\rangle_N |0\rangle_c . \tag{39}$$

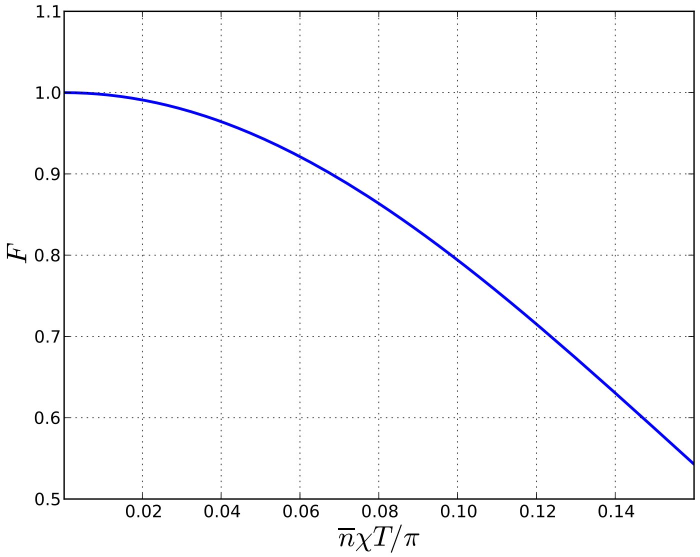

FIG. 5. Fidelity of un-conditional π rotation of the first two qubits of the initial state $|\alpha\rangle_c|\psi\rangle_4$ as a function of square pulse duration T. The cavity displacement is $\alpha = 2.5$ and the dispersive shift is $\chi/(2\pi) = 10\,\mathrm{MHz}$.

By resetting the cavity to the vacuum (via an ancilla qubit or a cavity Q-switch [26]) and repeating the procedure one generates the dissipative (non-unitary) evolution [14]

$$|0\rangle\langle 0|\otimes\rho_N \to |0\rangle\langle 0|\otimes\left(\boldsymbol{E}_0(\theta)\rho_N\boldsymbol{E}_0^\dagger(\theta)+\boldsymbol{E}_x^{(i)}(\theta)\rho_N\boldsymbol{E}_x^{(i)\dagger}(\theta)\right)\,, \tag{40}$$

with $\boldsymbol{E}_0(\theta) = \boldsymbol{P}_{S_M}^+ + \cos(\theta/2)\boldsymbol{P}_{S_M}^-$ and $\boldsymbol{E}_x^{(i)}(\theta) = i\sin(\theta/2)\boldsymbol{\sigma}_i^x\boldsymbol{P}_{S_M}^-$. Thus with probability $\sin^2(\theta/2)$, a -1 eigenstate of $\boldsymbol{Z}_{S_M}$ is converted into a $+1$ eigenstate. For $\theta = \pi$, this "stabilizer pumping" occurs with unit probability. Generalization to arbitrary weight-M Pauli-operators can be achieved with suitable single qubit rotations.

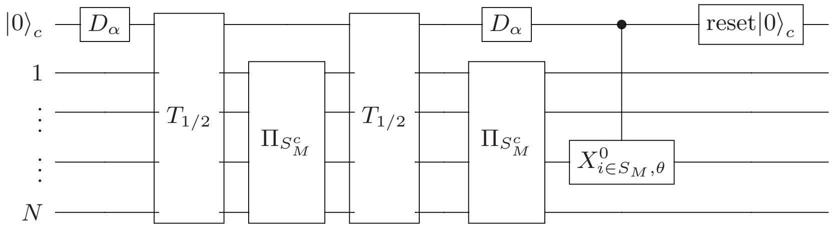

FIG. 6. Quantum circuit diagram for stabilizer pumping. D_α denotes an unconditional displacement by α. $T_{1/2}$ represents a free evolution of duration $T_{1/2} = \pi/4\chi$. $\Pi_{S_M^c}$ represents a (parallel) multi-qubit π-pulse on qubits in S_M^c. $X^0_{i\in S_M,\theta}$ represents a conditional rotation of qubit i by θ around the x-axis, conditioned on the cavity being in the vacuum. reset$|0\rangle_c$ represents the (dissipative) cavity reset operation.

DECOHERENCE

Decoherence due to photon losses and qubit decay and dephasing are treated within the Lindblad master equation formalism [33]. The master equation we solve numerically is

$$\dot\rho = -i[H,\rho]+\kappa\mathcal{D}[\boldsymbol{a}]\rho+\sum_i\left(\frac{\Gamma_\varphi}{2}\mathcal{D}[\boldsymbol{\sigma}_i^z]\rho+\Gamma_-\mathcal{D}[\boldsymbol{\sigma}_i^-]\rho++\Gamma_+\mathcal{D}[\boldsymbol{\sigma}_i^+]\rho\right)\,, \tag{41}$$

where $\mathcal{D}[\boldsymbol{L}]\rho = (2\boldsymbol{L}\rho\boldsymbol{L}^\dagger - \boldsymbol{L}^\dagger\boldsymbol{L}\rho - \rho\boldsymbol{L}^\dagger\boldsymbol{L})/2$. Here κ is the single photon decay rate of the cavity, Γ_φ is the phase relaxation (pure dephasing) rate of the qubits and the qubit relaxation rate is given by $1/T_1 = \Gamma_- + \Gamma_+$. We consider the zero-temperature limit $\Gamma_+ = 0$.

LOGICAL QUBIT STATE TOMOGRAPHY

In Fig. 3 of the main text, we show the state fidelity of the encoded logical qubit state to the target state $\exp[-i(\pi/8)\overline{X}]|\overline{0}\rangle$ as a function of the dispersive shift χ and cavity nonlinearity K. In the left panel of Fig. 7, we compare the resulting four-qubit state with the ideal target state in the Pauli-bar representation of the reduced density matrix (tracing out the cavity), for $K/(2\pi) = 80\,\mathrm{KHz}$, $\chi/(2\pi) = 5\,\mathrm{MHz}$ and $\kappa/(2\pi) = 10\,\mathrm{KHz}$. The fidelity to the target state is 94%. The right panel of Fig. 7 shows the Bloch-sphere representation of the prepared logical qubit state. From the latter, we see that the infidelity is due to both a loss of purity and a deviation from the ideal rotation.

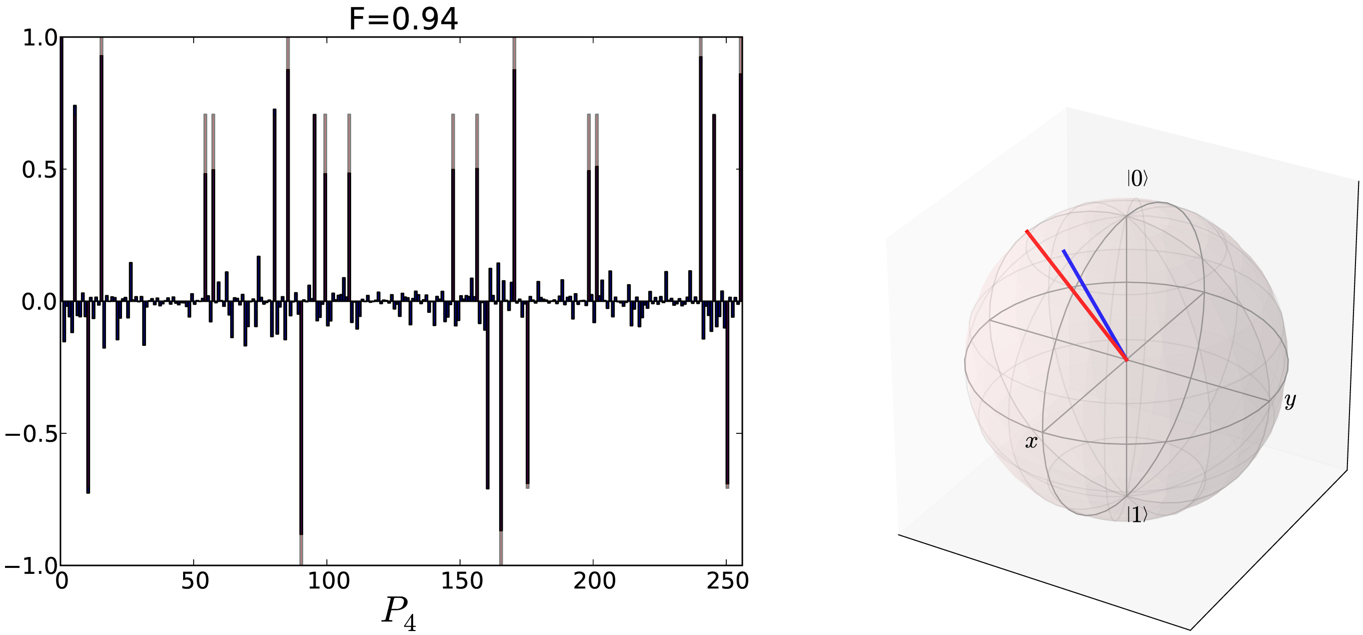

FIG. 7. (Color online) **Left panel:** Pauli-bar representation of the prepared four qubit state (full (blue) bars) and of the target state $\exp[-i(\pi/8)\overline{X}]|\overline{0}\rangle$ (lighter (red) bars). Here $\boldsymbol{P}_4 = \{\mathbb{1}, \boldsymbol{\sigma}^x, \boldsymbol{\sigma}^y, \boldsymbol{\sigma}^z\}^{\otimes 4}$ is the Pauli-group of order four. **Right panel:** Bloch-sphere representation of the prepared logical qubit state (full (blue) vector) and corresponding target state (full (red) vector).

DISCUSSION & OUTLOOK

We conclude these notes by an informal discussion of a few possible applications of our protocol to illustrate its versatility.

Implementation of the toric code

Because we can measure Pauli operators on arbitrary subsets of qubits, it becomes possible to implement "in software" non-trivial topologies such as required e.g. by the toric code [12], in which $2\mathfrak{g}$ logical qubits can be encoded into the ground state stabilizer subspace of a qubit manifold with genus $\mathfrak{g}$. Let us consider the case $\mathfrak{g} = 1$ of a ring torus as depicted in Fig. 8. The stabilizers of the $2N$-qubit toric code for example are the N plaquette $\boldsymbol{P}_i$ and N star

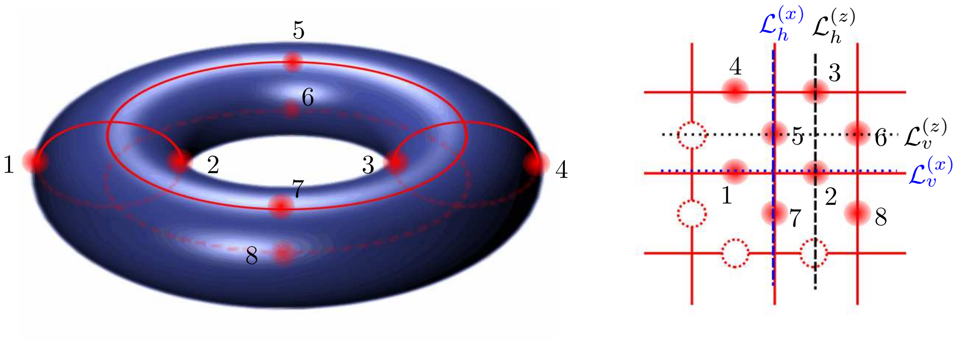

FIG. 8. **Left panel.** 8-qubit toric code. The qubits are represented by read beads. **Right panel.** Corresponding planar representation. The latter is easier to implement experimentally and the toric boundary conditions are imposed when defining the stabilizers. $\mathcal{L}_i^{(j)}$ indicate the incontractible loops used to define the logical qubit operators (see text).

operators $\boldsymbol{S}_i$ defined as

$$\boldsymbol{P}_i = \prod_{j\in\text{plaquette}_i} \boldsymbol{\sigma}_j^z\,, \quad \boldsymbol{S}_i = \prod_{j\in\text{star}_i} \boldsymbol{\sigma}_j^x\,. \tag{42}$$

Crucially, because of the toric boundary conditions it holds true that $\prod_{i\in\text{lattice}} \boldsymbol{P}_i = \prod_{i\in\text{lattice}} \boldsymbol{S}_i = \mathbb{1}$. These two constraints then lead to a four-fold degeneracy ($2^{2\mathfrak{g}}$-fold degeneracy in general) of the ground state manifold. A ground state of the toric code can be prepared by starting from the fully polarized state $|g,\ldots,g\rangle$ of the $2N$ qubits in the Z basis and sequentially measuring all the star operators and applying a corrective single qubit Z operation on a qubit in any star with eigenvalue -1. Fig. 8 illustrates a minimal 8-qubit toric code and its planar implementation. The stabilizers of this code are explicitly:

$$\begin{aligned}
\boldsymbol{P}_1 &= Z_1Z_4Z_7Z_8 & \boldsymbol{S}_1 &= X_1X_2X_5X_7\\
\boldsymbol{P}_2 &= Z_2Z_3Z_7Z_8 & \boldsymbol{S}_2 &= X_3X_4X_5X_7\\
\boldsymbol{P}_3 &= Z_1Z_4Z_5Z_6 & \boldsymbol{S}_3 &= X_1X_2X_6X_8\\
\boldsymbol{P}_3 &= Z_2Z_3Z_5Z_6 & \boldsymbol{S}_3 &= X_3X_4X_6X_8
\end{aligned} \tag{43}$$

Here $Z_i = \boldsymbol{\sigma}_i^z$ and $X_i = \boldsymbol{\sigma}_i^x$. Our protocol can also be used to measure the logical Pauli operators of the toric code, which are defined in terms of the incontractible X or Z loop operators winding the torus in either vertical or horizontal directions (see Fig. 8). Explicitly

$$\begin{aligned}
\overline{Z}^{(1)} &= \prod_{i\in\mathcal{L}_h^{(z)}} \boldsymbol{\sigma}_i^z & \overline{Z}^{(2)} &= \prod_{i\in\mathcal{L}_v^{(z)}} \boldsymbol{\sigma}_i^z\\
\overline{X}^{(1)} &= \prod_{i\in\mathcal{L}_v^{(x)}} \boldsymbol{\sigma}_i^x & \overline{X}^{(2)} &= \prod_{i\in\mathcal{L}_h^{(x)}} \boldsymbol{\sigma}_i^x\,.
\end{aligned} \tag{44}$$

Preparation of cluster states & measurement based quantum computation

Cluster states are the central resource of measurement based quantum computation [11]. A cluster state is a stabilizer state defined on a graph G, where each vertex i is associated with a stabilizer generator of the form $\boldsymbol{S}_i = X_i \prod_{j\in\text{nn}(i)} Z_j$ where $\text{nn}(i)$ denotes nearest neighbor vertices to vertex i. By applying a single qubit Hadamard rotation on qubit i at the beginning and at the end, we can use our encoding procedure to measure $\boldsymbol{S}_i$ and hence prepare arbitrary cluster states. To perform a quantum computation one requires in addition the ability to perform single-qubit measurements. Because single qubit operators are weight-one Pauli operators, we can again use our measurement protocol to perform such measurements and hence perform one-way measurement based quantum computation. In practice these single-qubit measurements can be done either as explained in the main text, by applying parallel echo π-pulses on all the qubits except the one being measured, or alternative by first performing a parity measurement of all the (appropriately rotated) qubits (i.e. without any echo π-pulses) yielding $P_{\text{tot}} \in \{\pm 1\}$ and then repeating the measurement, echoing-out only the qubit that is to be measured yielding $P^{(i)}_{\text{comp}} \in \{\pm 1\}$. The parity of the qubit to be measured is then given by $P_i = P_{\text{tot}}/P^{(i)}_{\text{comp}}$. The advantage of the latter approach is a drastic reduction in the number of necessary π-pulses (from $N-1$ to 1 where N is the total number of qubits). This reduction applies in general for subset parity measurements when the total number of qubits N is larger than twice the number of qubits in the subset M.

Conclusion

The proposed protocols offer a direct route to implement stabilizer quantum error correction and to "digitally simulate " models of topological quantum computation with superconducting qubits in the ultra-strong dispersive regime. From an experimental point of view, the main challenge presumably lies in engineering a system of multiple qubits with long coherence times and with sufficient separation of time scales to validate the approximations made in our derivations. A proof of principle experiment seems within reach of current technology.

As an outlook for future research, an interesting question is whether our approach can be extended to measure all stabilizers of a given code in parallel rather than sequentially. This should be possible in principle as these operators all commute with each other. A naive extension to encode an entire syndrome (collection of N stabilizers, each of which can have values ± 1) into 2^N-component cavity cat-states, would seem to require an unfortunate exponential increase in the required cat-size.